CHAPTER W9

Magnetic Properties of Materials

W9.1 Jahn–Teller Effect

Another effect that should be mentioned is the distortion of the octahedral arrangement of the six NN O^{2-} ions by $3d^4$ or $3d^9$ cations such as Mn^{3+} or Cu^{2+}, respectively. Due to the occupation of the $d_{x^2-y^2}$ and d_{z^2} atomic orbitals by the $3d$ electrons in these ions, additional asymmetric Coulomb forces will cause shifts in the positions of the cations and anions, thus producing additional tetragonal or octahedral distortions of the crystal. These distortions, which are a result of the *Jahn–Teller effect*, can remove the degeneracy of the lowest energy level. The Jahn–Teller effect corresponds to the removal of the ground-state degeneracy for a magnetic ion in a site of high symmetry by distortions of the structure which lower both the energy and the symmetry of the system. In the context of crystal field theory, the *Jahn–Teller theorem* states that such distortions are in fact expected to occur under certain specific conditions (e.g., when the symmetric ground state is not a *Kramers doublet* and when the effect is strong enough to dominate thermal effects and the effects of spin–orbit interaction).

W9.2 Examples of Weak and Strong Crystal Field Effects

The ionic complexes $Fe^{3+}(F^-)_6$ and $Fe^{3+}(CN^-)_6$ are examples of the weak- and strong-field limits, respectively, for the Fe^{3+} ion in an octahedral crystal field. In the former case the $3d^5$ Fe^{3+} ion has spin $S = \frac{5}{2}$, as expected from Hund's rules for a free ion, while in the latter case the Fe^{3+} spin $S = \frac{1}{2}$, corresponding to a single unpaired d electron. These values of the spin S are consistent with the predictions of crystal field theory presented in Table 9.2 of the textbook.[†] Crystal field theory is thus able to explain the variation in magnetic properties of the same ion in different crystal structures. In terms of the alternative molecular orbital theory, highly covalent bonding between the Fe^{3+} cation and the surrounding anions is proposed to occur in the strong-field $Fe^{3+}(CN^-)_6$ complex, while in the weak-field $Fe^{3+}(F^-)_6$ complex the bonding between cation and anions is primarily ionic with only a small covalent component.

W9.3 Crystal Fields and Cr^{3+} in Al_2O_3

The effects of crystal fields on a Cr^{3+} ion with a $3d^3$ electronic configuration in an octahedral site will now be considered in greater detail. Examples include Cr^{3+} in

[†] The material on this home page is supplemental to *The Physics and Chemistry of Materials* by Joel I. Gersten and Frederick W. Smith. Cross-references to material herein are prefixed by a "W"; cross-references to material in the textbook appear without the "W."

the solid antiferromagnetic oxide Cr_2O_3 or as an impurity or dopant ion in *ruby* (i.e., Al_2O_3), where each Cr^{3+} replaces an Al^{3+} ion. The latter example actually corresponds to the first solid-state material to exhibit laser action, as described in Chapter 18. In each of these examples six O^{2-} ions are the NNs of each Cr^{3+} ion. The free-ion ground state of the $3d^3$ Cr^{3+} ion is ${}^4F_{3/2}$ ($S = \frac{3}{2}$, $L = 3$, $J = L - S = \frac{3}{2}$) according to Hund's rules (see Table 9.1). The free-ion energy levels of Cr^{3+} and their splitting in an octahedral crystal field are shown in Fig. W9.1.†

The splitting of the energy levels of the Cr^{3+} ion by the crystal field is much larger than the splitting due to the spin–orbit interaction, not shown in Fig. W9.1, between free-ion energy levels with the same S and L but different J, (i.e., $J = L - S = \frac{3}{2}, \frac{5}{2}, \frac{7}{2}$, up to $J = L + S = \frac{9}{2}$. The ground-state ${}^4F_{3/2}$ configuration of the free Cr^{3+} ion, which is $(2S + 1)(2L + 1) = 28$-fold degenerate, is split into three levels in the crystal

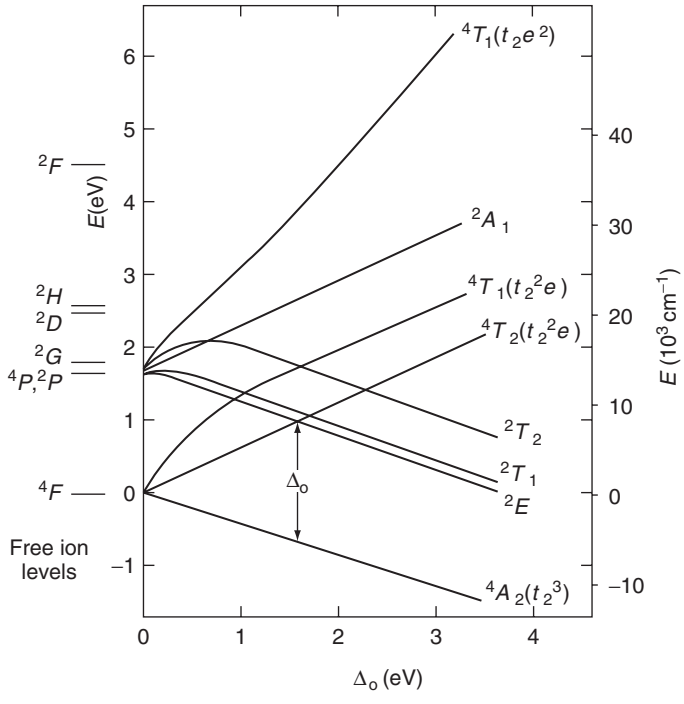

Figure W9.1. Free-ion energy levels of Cr^{3+} and their splitting in an octahedral crystal field shown in a Tanabe–Sugano diagram. The ground state of the $3d^3$ Cr^{3+} ion, ${}^4F_{3/2}$ ($S = \frac{3}{2}$, $L = 3$, $J = L - S = 3/2$), is split into three levels in the crystal field: a lower ${}^4A_2$ level and two upper levels, ${}^4T_2$ and ${}^4T_1$. The value $\Delta_o \approx 1.8$ eV for Cr^{3+} in Al_2O_3 is obtained from optical absorption spectroscopy.

† Energy-level diagrams known as Tanabe–Sugano diagrams for ions with $3d^n$ configurations in both octahedral and tetrahedral crystal fields are shown as functions of crystal field strength in Sugano et al. (1970, pp. 108–111). The transitions from the high-spin state ($\Delta_o < U$) to a state with lower spin ($\Delta_o > U$) are shown in these diagrams to occur at critical values of Δ_o for ions with $3d^4$, $3d^5$, $3d^6$, and $3d^7$ configurations.

TABLE W9.1 Mulliken Symbols for Crystal Field Representations[a]

Symbol M	Dimensionality	Symmetry
A	One	Symmetric with respect to rotation by $2\pi/n$ about the principal C_n axis.
B	One	Antisymmetric with respect to rotation by $2\pi/n$ about the principal C_n axis.
E	Two	
T	Three	
g (subscript)	—	Attached to symbols for representations that are symmetric with respect to inversion
e (subscript)	—	Attached to symbols for representations that are antisymmetric with respect to inversion

[a]For additional details, see F. A. Cotton, *Chemical Application of Group Theory*, 3rd ed., Wiley-Interscience, New York, 1990, p. 90.

field, a lower fourfold degenerate $^4A_2$ level and two upper levels, $^4T_2$ and $^4T_1$, each of which is 12-fold degenerate. These new levels in the crystal field are denoted by the group-theoretic labels ^{2S+1}M, where M refers to the *Mulliken notation*. The meanings of the Mulliken symbols are summarized briefly in Table W9.1.

Note that L is no longer a good quantum number in the presence of the crystal field and so can no longer be used to designate the new levels. The $^4A_2$ level remains the lowest energy level for all crystal field strengths, and therefore a high-spin to low-spin transition is not observed for Cr^{3+} in octahedral crystal fields, as expected from Table 9.2.

The crystal field splittings Δ_o of the energy levels of the Cr^{3+} ion are also typically larger than splittings due to the Coulomb interaction between free-ion levels with different L (e.g., between the $^4F_{3/2}$ ground state and the ^4P, ^2P, ^2G, ^2D, ^2H, and ^2F excited states shown in Fig. W9.1). As a result of crystal field splitting, the ground state of the ion is no longer $(2L + 1) =$ sevenfold orbitally degenerate. Instead, orbitals with different values of m_l now have different energies in the solid. The splitting of the ground-state level in a magnetic field therefore lifts only the degeneracy due to the spin S. As a result, the ion acts magnetically as if $J = S$, with an effective magneton number $p = g\sqrt{S(S+1)}$. This is consistent with the p observed for Cr^{3+}, presented in Table 9.1.

The value of the crystal field splitting Δ_o (often referred to in the literature as $10Dq$) for Cr^{3+} in Al_2O_3 has been obtained from optical spectroscopy. The optical absorption spectrum observed for Al_2O_3 containing Cr^{3+} as an impurity cannot be explained as being due to absorption by the Al_2O_3 host or to transitions between energy levels in the free Cr^{3+} ion. Instead, the absorption is due to transitions between the new energy levels of the Cr^{3+} ion in the octahedral crystal field. The specific transitions involved are from the ground-state $^4A_2$ level to the excited-state levels shown in Fig. W9.1, including the ^2E, $^2T_1$, $^4T_2$, $^2T_2$, and $^4T_1$ levels. The value $\Delta_o = 1.8$ eV is obtained in this way. These energy levels for the Cr^{3+} ion lie within the energy gap of the Al_2O_3 host, as is often the case for transition metal impurities in insulating materials.

The crystal field quenches the orbital angular momentum L by splitting the originally orbitally degenerate levels into levels separated by energies that are much greater than mH, where m is the magnetic moment of the atom or ion. In this case the magnetic field can split the spin-degenerate levels of the ground state only into the $(2S + 1)$ nondegenerate levels, which are responsible for the paramagnetic susceptibility of the ion, discussed in more detail in Section 9.4.

W9.4 Experimental Results for χ in the Free-Spin Limit

Experimental results[†] for the contribution of Mn spins to the low-field magnetic susceptibility χ of a series of six dilute alloys of Mn in Au are shown in Fig. W9.2, plotted in this case as χ versus T/n on a logarithmic plot. The fact that Mn impurities at dilute concentrations tend to act as free spins in Au is clear since the measured values of χ for the six alloys lie close to a single straight line with a slope of -1, consistent with Curie law behavior. Note also that since the measured values of $\chi = M/H$ are much less than 1, it follows that $M \ll H$. This justifies the use of the approximation $B = \mu_o H$. Assuming that $g = 2$, the value of the magnitude of the spin for Mn in Au obtained from the Curie constant C is $S = 2.25 \pm 0.1$, which is close to the Mn^{2+} free-ion value of $S = 2.5$ (see Table 9.1). This value of S is the same as that obtained from the measured saturation magnetization for the same alloys, using $S = M_{sat}/ng\mu_B$.

Evidence for the appearance of interactions at high n and low T can be seen in Fig. W9.2 where χ at low T for the highest-concentration AuMn alloy falls below the straight line that represents the Curie law behavior observed for the lower-concentration

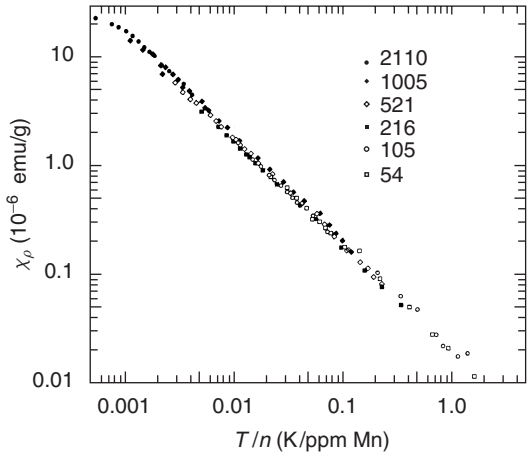

Figure W9.2. Experimental results for the contribution of Mn spins to the low-field magnetic susceptibility χ of a series of six dilute alloys of Mn in Au are shown plotted as χ versus T/n on a logarithmic plot. The concentration n of Mn spins is given in parts per million (ppm). [From J. C. Liu, B. W. Kasell, and F. W. Smith, *Phys. Rev. B*, **11**, 4396 (1975). Copyright © 1975 by the American Physical Society.

[†] J. C. Liu, B. W. Kasell, and F. W. Smith, *Phys. Rev. B*, **11**, 4396 (1975).

alloys. This result indicates that the spins in the most concentrated alloy are not as "susceptible" as free spins in their response to external magnetic fields. Instead, their coupling to and interaction with each other limits their ability to respond to external fields and hence lowers their susceptibility χ. The type of interaction responsible for this behavior in AuMn alloys is an indirect interaction mediated by the conduction electrons.

W9.5 Spin Glasses and the RKKY Interaction

Clear evidence for the existence of the RKKY interaction has been found from studies of the magnetic properties of dilute alloys (e.g., Mn in Au, Ag, Cu, and Zn). When the spins of magnetic Mn^{2+} ions are coupled to each other via the conduction electrons, the average energy of the spin–spin interaction $\langle U_{\mathrm{RKKY}} \rangle$ is given by nV_0, where n is the concentration of Mn^{2+} ions per unit volume. This energy of interaction between spins competes with the energy of thermal disorder $k_B T$, with the result that the free-spin Curie law $\chi(T) = C/T$ is modified and becomes instead

$$\chi(T) = \frac{C}{T + \theta}. \tag{W9.1}$$

Here C is again the Curie constant as defined in Eq. (9.26) and $\theta \approx nV_0/k_B > 0$ is the Curie–Weiss temperature.[†] Equation (W9.1) is known as the *Curie–Weiss law* for the magnetic susceptibility and is valid for $T \gg \theta$ (i.e., for $k_B T \gg nV_0$).

Note that $\chi(T) = C/(T + \theta)$ with $\theta > 0$ is smaller than the free-spin susceptibility $\chi(T) = C/T$ for all T, indicating again that spin–spin interactions reduce the ability of the interacting spins to respond to external magnetic fields. This behavior has already been illustrated in Fig. W9.2, where, as stated previously, χ for the highest-concentration AuMn alloy at low T falls below the straight line that represents the Curie law behavior observed at higher T .

As $T \to \infty$ the Curie and Curie–Weiss laws become essentially identical since thermal fluctuations will always overcome magnetic interactions in this limit. The most significant difference is found for $T \ll \theta$, where $\chi(T) = C/(T + \theta)$ reaches a finite value while $\chi(T) = C/T$ for free spins diverges as $T \to 0$. The dependence of χ on T expressed by the Curie–Weiss law in Eq. (W9.1) is also observed in ferromagnetic and antiferromagnetic materials in their paramagnetic states above their respective critical temperatures T_c. For ferromagnets it is found that $\theta < 0$, whereas for antiferromagnets $\theta > 0$.

W9.6 Kondo Effect and s–d Interaction

One more interesting effect involving localized spins and the conduction electrons in metals can be mentioned. At sufficiently low temperatures the s–d or exchange interaction given in Eq. (9.32) can lead to a complicated many-body ground state of the system of the spin $\boldsymbol{S}$ and the conduction electrons of the metal. As already mentioned, the scattering of an electron from a magnetic ion can cause the spin of the scattered electron to flip (i.e., to change its direction), with a compensating change

[†] A. I. Larkin and D. E. Khmel'nitskii, *Sov. Phys. JETP*, **31**, 958 (1970).

TABLE W9.2 Competing Effects for Localized Spins in Metals: Thermal, RKKY, and Kondo Effects

$nV_0 \gg k_BT_K$: spin–spin interactions are dominant.	
$k_BT \gg nV_0$	Free spins
$k_BT \ll nV_0$	Frozen spins (spin glass behavior)
$k_BT_K \gg nV_0$: single-spin effects are dominant.	
$T \gg T_K$	Free spins
$T \ll T_K$	Compensated spins

occurring in the direction of the localized spin. The onset of this new ground state is typically signaled by the appearance of a minimum in the resistance of the metal as the temperature is lowered. It has been predicted that below a characteristic temperature T_K the spin $\boldsymbol{S}$ of the magnetic ion will be effectively canceled or compensated by the oppositely directed spins of the conduction electrons that interact with $\boldsymbol{S}$. This behavior is known as the *Kondo effect*, and the magnitude of the *Kondo temperature* T_K increases as the strength of the s–d interaction increases.

The s–d interaction, if sufficiently strong, can lead to complete mixing of the conduction electrons and the localized d electrons of the magnetic ion and therefore to the disappearance of the localized spin S. An example of this behavior is provided by Mn^{2+} ions, which do not retain well-defined magnetic moments in certain dilute alloys such as Mn in Al. In this case the characteristic temperature T_K for the s–d interaction is apparently very high, ≈ 1000 K, since for $T < T_K$, the spin will be compensated and hence effectively absent.

The three competing effects that ultimately determine the behavior and possibly even the existence of localized spins in metals are thermal effects, effects due to the spin–spin RKKY interaction, and the single-spin Kondo effect.[†] The characteristic energies that determine the strengths of these three effects are k_BT, nV_0, and k_BT_K, respectively. The possible regimes of behavior are defined in terms of the relative magnitudes of these three energies in Table W9.2. It can be seen that free-spin behavior should in principle always be observed in solids at sufficiently high T. The term *spin glass* used in the table is defined in the discussion of magnetism in disordered materials in Section W9.11.

W9.7 $\chi(T)$ for Ni

A test of the Curie–Weiss law $\chi(T) = C/(T - T_C)$ for the ferromagnet Ni is shown in Fig. W9.3, where χ_ρ^{-1} is plotted as a function of T. It can be seen that significant deviations from Curie–Weiss behavior occur just above $T_C = 627$ K. It is found experimentally for Fe that χ is proportional to $(T - T_C)^{-\gamma}$ as $T \to T_C$ from above. Here γ is measured to be 1.33 instead of the value 1 predicted by the Curie–Weiss law. The molecular field theory fails near T_C since it does not include the effects of fluctuations of the local magnetization.

[†] An alternative approach to the question of the existence of localized spins in metals has been developed by Anderson (P. W. Anderson, Phys. Rev., **124**, 41 (1961) and by Wolff (P. A. Wolff, Phys. Rev., **124**, 1030 (1961).) For a useful discussion of this approach, see White and Geballe (1979).

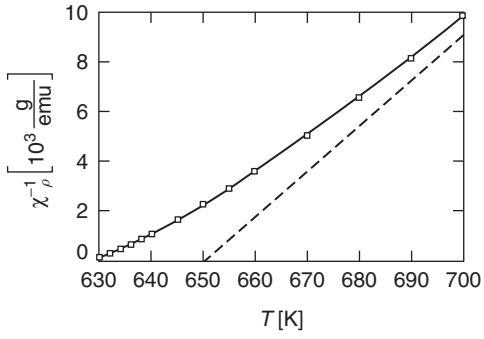

Figure W9.3. Test of the Curie–Weiss law $\chi(T) = C/(T - T_C)$ for the ferromagnet Ni in the form of a plot of χ_ρ^{-1} as a function of T . Deviations from Curie–Weiss behavior are observed just above $T_C = 627$ K. The straight line is the extrapolation of the results obtained for $T > 700$ K and is given by $\chi(T) = C/(T - \theta)$ where $\theta = 650$ K. [Data From J. S. Kouvel et al., *Phys. Rev.*, **136**, A1626 (1964).]

W9.8 Hubbard Model

An approach that attempts to include both itinerant and localized effects and also electron correlations within the same model is based on a proposal by Hubbard.[†] In the *Hubbard model* the oversimplified view is taken that the electrons in the partially filled shell of the free ion enter a single localized orbital in the solid. There are two important energies in the Hubbard model. The *Coulomb repulsion energy* $U > 0$ represents the effects of electron correlations between pairs of opposite-spin electrons occupying the same orbital on a given ion, and the *hopping* or *tunneling energy* is t. The parameter t is effectively the matrix element between states on neighboring ions which differ by one electron of a given spin direction and is therefore related to the energy required for an electron to hop from one site (i.e., one ion) to one of its NNs without changing its spin direction. In a one-state Hubbard model there is one orbital per atom and each orbital can be occupied by electrons in four different ways: (1) the orbital is empty: $(-,-)$, (2) and (3) the orbital is occupied by either a spin-up or a spin-down electron: $(\downarrow, -)$ or $(-,\uparrow)$, or (4) the orbital is doubly occupied: $(\downarrow,\uparrow)$.

In the limit $U \gg t$ and when there are just as many electrons as ions, there will be a strong preference for occupation of each orbital by a single electron (i.e., case 2 or 3 above). This limit corresponds to an antiferromagnetic insulator in which the effective exchange integral is $J = -4t^2/U$, with adjacent orbitals occupied by opposite spin electrons. In the opposite limit of $U \ll t$, the electrons are not localized but instead, form a band of itinerant electrons. Thus the Hubbard model is capable of describing a wide range of magnetic behavior in solids, depending on the relative values of the two parameters U and t. In addition, the Hubbard model has the advantage that it can be formulated so that the condition for local magnetic moment formation is not the same as that for the occurrence of long-range order in the spin system. The negative-U limit of the Hubbard model has been applied to charged defects in semiconducting and insulating solids. The defect is negatively charged when the orbital in question is

[†] J. Hubbard, *Proc. R. Soc.* A, **276**, 238 (1963); **277**, 237 (1964); **281**, 401 (1964).

doubly occupied, or positively charged when the orbital is unoccupied. The energy U can be effectively negative when lattice relaxations occur that favor negatively charged defects.

The Hubbard model goes beyond the one-electron tight-binding approximation presented in Chapter 7, in that it includes electron–electron interactions when two electrons reside on the same site. The application of the Hubbard model to high-T_c oxide-based superconductors is described briefly Chapter W16.

W9.9 Microscopic Origins of Magnetocrystalline Anisotropy

The microscopic origins of magnetocrystalline anisotropy can be viewed as arising from anisotropic interactions between pairs of spins when these interactions are significant and also from the interaction of a single spin with its local atomic environment (i.e., the crystal field). The *pair model* of Van Vleck, developed in 1937, attempts to explain the change of the energy of interaction of pairs of spins according to their directions relative to their separation $\mathbf{r}$. This type of interaction is called *anisotropic exchange*, in contrast to the isotropic Heisenberg exchange interaction of Eq. (9.30). The spin–orbit interaction is believed to be an important source of the magnetic anisotropy. In the pair model the first-order anisotropy coefficient K_1 is predicted to be proportional to a high power of the spontaneous magnetization M_s in the ferromagnet. This result can explain the observed rapid decrease of K_1 with increasing temperature, with M_s and K_1 both falling to zero at T_C.

The direction of the spin of a magnetic ion in a material can also depend on the nature of the crystal field acting on the ion. In this way the local atomic environment can influence the direction of the magnetization M, hence giving rise to anisotropy. In fact, the electronic energy levels of the ion are often modified by the interaction with the crystal field, as discussed in Section 9.3.

W9.10 $\chi_\parallel$ and $\chi_\perp$ for Antiferromagnetic Materials

The predicted differences between $\chi_\parallel$ and $\chi_\perp$ discussed in the textbook are clear evidence that the magnetic properties of antiferromagnetic materials can be expected to be anisotropic below T_N. For example, in MnO the preferred directions for the sublattice magnetizations $\boldsymbol{M}_{sA}$ and $\boldsymbol{M}_{sB}$, and hence the directions corresponding to $\chi_\parallel$, can be seen from Fig. 9.17 to be the $[\bar{1}01]$ and $[10\bar{1}]$ directions in the {111} planes. Also, if an antiferromagnet were perfectly isotropic below T_N, it would follow that $\chi_\parallel = \chi_\perp$. Since $\chi_\perp > \chi_\parallel$ for $T < T_N$, it can be energetically favorable for the spins to rotate so that the spin axis is perpendicular to the applied field. This "flopping" of the spin axis occurs at a critical applied magnetic field which is determined by the relative strengths of the magnetocrystalline anisotropy and the antiferromagnetic interactions.

W9.11 Magnetism in Disordered Materials

Spin glasses (i.e., dilute magnetic alloys) are the focus of this section, due to the fairly simple, yet important ideas involved in the explanation of their magnetic behavior. In general, nonuniform internal molecular fields $\mathbf{B}_{\text{eff}}$ whose magnitudes and directions vary from spin to spin are present in amorphous magnetic materials. The probability distribution $P(\mathbf{B}_{\text{eff}})$ of the magnitudes of these internal fields in spin glasses (e.g.

$Cu_{0.99}Fe_{0.01}$) will be nonzero even at $B_{\text{eff}} = 0$. Thus there will always be spins with $B_{\text{eff}} = 0$ which are effectively free to respond to thermal excitations and to external magnetic fields. This is clearly not the case in the magnetically ordered materials discussed in the textbook, in which every spin experiences a nonzero molecular field, at least below the critical temperature T_C or T_N for magnetic ordering.

In sufficiently dilute spin glasses and at relatively high temperatures each spin can in principle be thought of as being free or as interacting with at most one other spin in the material. The spins typically interact via the indirect RKKY interaction through the conduction electrons. In this case the contributions of the interacting spins to the magnetization M, the magnetic susceptibility χ, and the magnetic contribution C_M to the specific heat obey the following *scaling laws* involving temperature T and magnetic field H:

$$\begin{aligned} \frac{M(H,T)}{n} &= F_M\left(\frac{T}{n}, \frac{H}{n}\right), \\ \chi(T) &= F_\chi\left(\frac{T}{n}\right), \\ \frac{C_M(T)}{n} &= F_C\left(\frac{T}{n}\right). \end{aligned} \tag{W9.2}$$

Here n is the concentration of magnetic impurities, and F_M, F_χ, and F_C are functions only of H and T through the reduced variables H/n and T/n. These scaling laws follow from the $1/r^3$ dependence of the RKKY interaction on the separation r between spins, as presented in Eqs. (9.33) and (9.34).

Since the average separation $\langle r \rangle$ between randomly distributed spins can be approximated by $n^{-1/3}$, it follows that the average strength $\langle J_{\text{RKKY}}(r) \rangle$ of the interaction between spins is proportional to $\langle V_0/r^3 \rangle$ (i.e., to nV_0), where V_0 is a constant for a given combination of magnetic impurity and host material. The value for V_0 in dilute CuMn alloys[†] is $V_0 = 7.5 \times 10^{-50}$ J $\cdot$ m^3. Taking a Mn concentration of 0.1 at % = 1000 parts per million (ppm) in Cu yields $n = 8.45 \times 10^{25}$ Mn spins/m^3 and $nV_0 = 6.3 \times 10^{-24}$ J $\approx 4 \times 10^{-5}$ eV. This concentration corresponds to an average distance between Mn spins of about 2 nm. The value of J_{sd} for CuMn can be obtained from Eq. (9.35) using the result given above for V_0, a density of states for Cu of $\rho(E_F) = 2.34 \times 10^{47}$ J^{-1}m^{-3}. The value so obtained is $J_{sd} = 3.45 \times 10^{-19}$ J $= 2.16$ eV.

The scaling behavior of $\chi(T)$ predicted above has already been demonstrated in Fig. W9.2, where χ is shown plotted as a function of T/n for several AuMn alloys. The measured magnetization M for three of these AuMn alloys at a fixed value of T/n is shown in Fig. W9.4 plotted as M/n versus H/n. The scaling behavior predicted is again observed. The magnetization $M(H)$ shown here falls well below the corresponding Brillouin function $M = ng\mu_B J B_J(g\mu_B JB/k_B T)$, which would apply if the spins were free (i.e., completely noninteracting).

Experimental results for the magnetic contribution C_M to the specific heat of a series of dilute alloys of Mn in Zn are shown in Fig. W9.5, where C_M/n is plotted as a function of T/n. Scaling is observed for the more-concentrated alloys where RKKY

[†] F. W. Smith, *Phys. Rev. B*, **14**, 241 (1976).

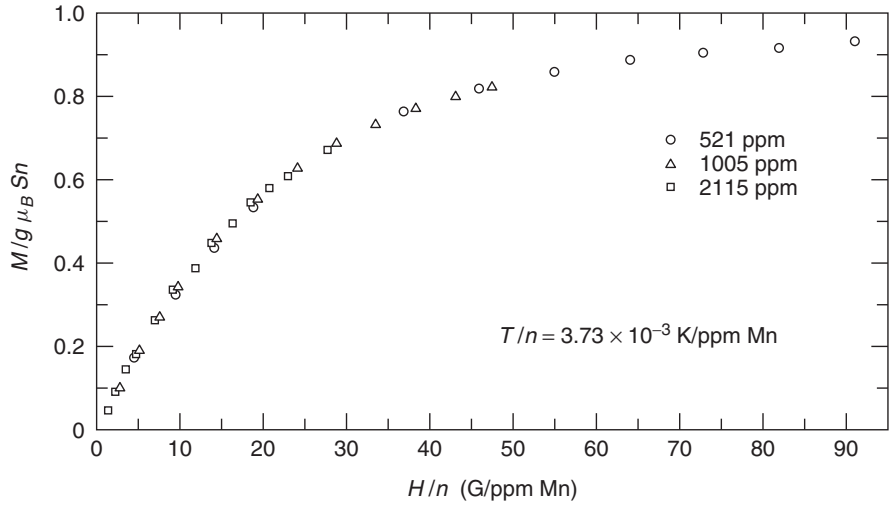

Figure W9.4. Contribution of the Mn spins to the magnetization M for three dilute alloys of Mn in Au at a fixed value of T/n plotted as $M/g\mu_B Sn$ versus H/n. The predicted scaling behavior $M(T)/n = F_M(H/n)$ is observed. [From J. C. Liu, B. W. Kasell, and F. W. Smith, *Phys. Rev. B*, **11**, 4396 (1975). Copyright © 1975 by the American Physical Society.

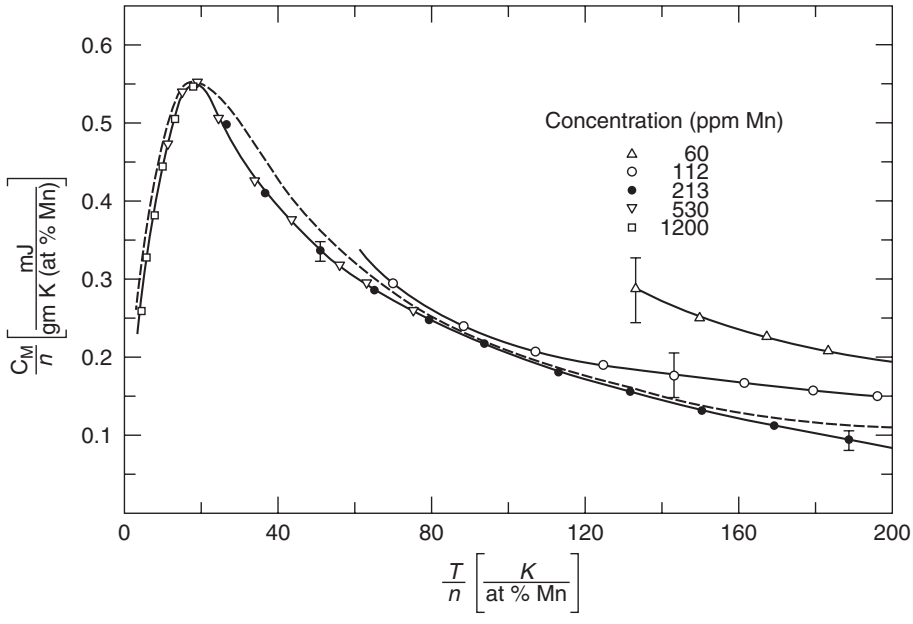

Figure W9.5. Experimental results for the magnetic contribution C_M to the specific heat of a series of dilute alloys of Mn in Zn, with C_M/n plotted as a function of T/n. Scaling is observed for the more concentrated alloys. [From F. W. Smith, *Phys. Rev. B*, **9**, 942 (1974). Copyright © 1974 by the American Physical Society.]

interactions dominate, whereas evidence for single-impurity effects, possibly due to the Kondo effect, is observed for the more dilute alloys at higher values of T/n. The peak observed in the measured specific heat at $T/n \approx 20$ K/(at % Mn) corresponds to a value of the ratio $k_B T/nV_0$ of thermal to RKKY interaction energies approximately equal to 2. At lower T (i.e., for $k_B T < nV_0$) interactions between the spins cause them to "freeze" in the local molecular field due to their neighboring spins. At $T = 0$ K the spin glass is magnetically "frozen" and the spins are oriented along the direction of their local molecular field. As T is lowered it is found experimentally that $C_M \propto n^2$, indicating that interactions first appear between pairs of spins. The typical size of an interacting cluster of spins increases as T decreases or n increases until the interactions extend throughout the entire spin system.

The magnetic behavior of dilute spin glasses can thus be understood as resulting from RKKY interactions between pairs of spins. Evidence for clusters of spins can be found in more concentrated spin glasses, such as Cu containing more than a few atomic percent Mn or in alloys such as Cu_xNi_{1-x} and Fe_xAl_{1-x}. Although the magnetic behavior is much more complicated in these concentrated alloys, the RKKY interaction still plays an important role. The term *mictomagnetism* is sometimes used to describe such materials in which the orientations of the spins are disordered and frozen at low temperatures.

REFERENCES

Sugano, S., Y. Tanabe, and H. Kamimura, *Multiplets of Transition-Metal Ions in Crystals*, Academic Press, San Diego, Calif., 1970.

White, R. M., and T. H. Geballe, *Long Range Order in Solids*, Suppl. 15 of H. Ehrenreich, F. Seitz, and D. Turnbull, eds., *Solid State Physics*, Academic Press, San Diego, Calif., 1979.

PROBLEMS

W9.1 Using Hund's rules, find the values of S, L, and J for the atoms in the $4d$ transition element series (Y to Pd). Compare these values with the corresponding results given in Table 9.1 for the $3d$ series.

W9.2 From Fig. 9.5 it can be seen that, relative to the degenerate spherically symmetric level, the d_{xy}, d_{yz}, and d_{xz} orbitals are shifted lower in energy by $2\Delta_o/5$ for the octahedral case and higher in energy by $2\Delta_t/5$ for the tetrahedral case. The corresponding opposite shifts for the $d_{x^2-y^2}$ and d_{z^2} orbitals are by the amount $3\Delta_o/5$ or $3\Delta_t/5$ for the octahedral and tetrahedral cases, respectively. Show that these energy shifts are such that the total energy of the $3d^{10}$ configuration will be the same in both the spherically symmetric and crystal-field-split cases.

W9.3 Using the schematic energy-level diagrams shown in Fig. 9.5, calculate the crystal field stabilization energies (CFSEs) and spins S [assuming that orbital angular momentum L is quenched (i.e., $L = 0$)]:

(a) For the $3d^n$ ions in octahedral sites. Compare your results with the values presented in Table 9.2.

(b) For the $3d^n$ ions in tetrahedral sites.

(c) In a ferrite such as Fe_3O_4, will Fe^{2+} ions prefer to enter octahedral or tetrahedral sites on the basis of their crystal field stabilization energy CFSE? What about Fe^{3+} ions?

W9.4 Show that the induced saturation magnetization M_{sat} for a system of $n = 10^{26}/\text{m}^3$ free spins in a material makes a negligible contribution to the magnetic induction B .

W9.5 Derive the general expression for the Brillouin function $B_J(x)$ given in Eq. (9.24).

W9.6 Consider a dilute magnetic alloy that contains $n = 2 \times 10^{23}$ spins/m^3. At low T the spins can be saturated in a field $H \approx 4 \times 10^6$ A/m, with M_{sat} measured to be 5.56 A/m. At high T the spins obey a Curie–Weiss law $\chi(T) = C/(T + \theta)$ with Curie constant $C = 7.83 \times 10^{-6}$ K and Curie–Weiss temperature $\theta = 0.1$ K.

(a) From these data determine the spin J and g factor of the spins.

(b) Are the spins free? If not, what type of spin–spin interaction would you conclude is present in the alloy?

W9.7 Consider a spin S in a ferromagnet interacting only with its z NN spins ($z = 12$ for an FCC lattice).

(a) Using Eq. (9.41) show that the Curie–Weiss temperature θ is given by $\theta = zS(S + 1)J(\mathbf{R}_{NN})/3k_B$, where the exchange integral $J(r)$ is evaluated at the NN distance $\mathbf{R}_{NN}$.

(b) Using the approximate values $\theta \approx T_C = 1043$ K and $S \approx 1$ for BCC ferromagnetic α-Fe, calculate the value of $J(\mathbf{R}_{NN})$.

W9.8 Show that at the Néel temperature T_N, the predicted maximum value for the magnetic susceptibility χ according to the molecular field model is $\chi_{\text{max}} = -1/\lambda_{\text{AB}} > 0$. Explain why this prediction that χ_{max} is proportional to $1/\lambda_{\text{AB}}$ is physically reasonable.

W9.9 Calculate the Pauli paramagnetic susceptibility χ_P for Na metal according to the free-electron theory.